NeuroImage 169 (2018) 46–56

Contents lists available at ScienceDirect

NeuroImage

journal homepage: www.elsevier.com/locate/neuroimage

Perturbation of whole-brain dynamics *in silico* reveals mechanistic differences between brain states

Gustavo Deco [a,b,c,d,**], Joana Cabral [e,f,g], Victor M. Saenger [a], Melanie Boly [h,i], Enzo Tagliazucchi [j,k], Helmut Laufs [k,l], Eus Van Someren [m,n], Beatrice Jobst [a], Angus Stevner [e,f], Morten L. Kringelbach [e,f,g,o,*]

[a] Computational Neuroscience Group, Center for Brain and Cognition, Universitat Pompeu Fabra, Barcelona, Spain
[b] Institució Catalana de la Recerca i Estudis Avançats (ICREA), Barcelona, Spain
[c] Department of Neuropsychology, Max Planck Institute for Human Cognitive and Brain Sciences, Leipzig, Germany
[d] School of Psychological Sciences, Monash University, Clayton, Melbourne, Australia
[e] Department of Psychiatry, University of Oxford, Oxford, UK
[f] Center for Music in the Brain, Department of Clinical Medicine, Aarhus University, Denmark
[g] Life and Health Sciences Research Institute (ICVS), School of Medicine, University of Minho, Braga, Portugal
[h] Department of Psychiatry, University of Wisconsin-Madison, Wisconsin, USA
[i] Department of Neurology, University of Wisconsin-Madison, Wisconsin, USA
[j] Institute for Medical Psychology, Christian Albrechts University, Kiel, Germany
[k] Department of Neurology and Brain Imaging Center, Goethe University, Frankfurt am Main, Germany
[l] Department of Neurology, Christian Albrechts University, Kiel, Germany
[m] Department of Sleep and Cognition, Netherlands Institute for Neuroscience, An Institute of the Royal Netherlands Academy of Arts and Sciences, Amsterdam, Netherlands
[n] Departments of Integrative Neurophysiology and Psychiatry GGZ InGeest, Center for Neurogenomics and Cognitive Research, VU University and Medical Center, Amsterdam, Netherlands
[o] Institut d'études avancées de Paris, France

ARTICLE INFO

Keywords:
Brain state
Sleep
Whole brain modeling
Perturbation

ABSTRACT

Human neuroimaging research has revealed that wakefulness and sleep involve very different activity patterns. Yet, it is not clear why brain states differ in their dynamical complexity, e.g. in the level of integration and segregation across brain networks over time. Here, we investigate the mechanisms underlying the dynamical stability of brain states using a novel off-line *in silico* perturbation protocol. We first adjust a whole-brain computational model to the basal dynamics of wakefulness and deep sleep recorded with fMRI in two independent human fMRI datasets. Then, the models of sleep and awake brain states are perturbed using two distinct multifocal protocols either promoting or disrupting synchronization in randomly selected brain areas. Once perturbation is halted, we use a novel measure, the Perturbative Integration Latency Index (PILI), to evaluate the recovery back to baseline. We find a clear distinction between models, consistently showing larger PILI in wakefulness than in deep sleep, corroborating previous experimental findings. In the models, larger recoveries are associated to a critical slowing down induced by a shift in the model's operation point, indicating that the awake brain operates further from a stable equilibrium than deep sleep. This novel approach opens up for a new level of artificial perturbative studies unconstrained by ethical limitations allowing for a deeper investigation of the dynamical properties of different brain states.

Introduction

Investigating brain function often requires using a black box approach, from which information can be obtained by: 1) measuring the spontaneous activity arising from the non-perturbed system; or 2) perturbing the system and measuring how the system responds. This information then serves to postulate mechanistic scenarios, which may be verified via mathematical/computational models. In the case of

* Corresponding author. Department of Psychiatry, University of Oxford, Oxford, UK.
** Corresponding author. Universitat Pompeu Fabra, C/ Ramon Trias Fargas, 25-27, 08005 Barcelona, Spain.
E-mail addresses: gustavo.deco@upf.edu (G. Deco), morten.kringelbach@psych.ox.ac.uk (M.L. Kringelbach).

https://doi.org/10.1016/j.neuroimage.2017.12.009
Received 1 June 2017; Received in revised form 27 November 2017; Accepted 4 December 2017
Available online 7 December 2017

perturbation, a wide range of schemes is available, ranging from natural interventions such as sensory stimuli or task instructions, to artificial - usually electromagnetic - interventions such as transcranial magnetic stimulation (TMS) or deep brain stimulation (DBS).

Alterations in brain activity elicited by natural perturbations can be detected non-invasively and at the whole-brain level using functional MRI (fMRI), allowing to map the brain regions whose activity correlates with different stimuli or tasks, resulting in a detailed repertoire of task-specific functional networks (Rissman et al., 2004; Raichle, 2009; Yarkoni et al., 2011). Notably, many of these task-specific functional networks have also been detected in baseline brain activity during rest (Biswal et al., 1995; Raichle et al., 2001; Damoiseaux et al., 2006; Smith et al., 2009; Zhang and Raichle, 2010). With hindsight, the fact that the brain at rest still exhibits highly structured spatiotemporal patterns of activity has important implications for our understanding of brain function (Raichle et al., 2001; Deco et al., 2011; Cabral et al., 2014; Cole et al., 2014; Deco and Kringelbach, 2016).

Beyond the insights obtained under natural conditions, direct artificial perturbations allow for the systematic exploration of dynamical responses elicited by controlled perturbative protocols. However, such perturbative approaches are generally limited to TMS in healthy humans (Siebner et al., 2009), or DBS in human patients, due to ethical considerations (Kringelbach et al., 2007b; Clausen, 2010; Kringelbach and Aziz, 2011; Fox et al., 2014). Combining these direct stimulation techniques with whole-brain neuroimaging allows exploring how the system leaves the resting equilibrium by characterizing the resulting dynamics in terms of complexity and latencies using TMS-EEG (Ilmoniemi et al., 1997; Massimini et al., 2005; Litvak et al., 2007; Casali et al., 2013), DBS-MEG (Kringelbach et al., 2007a; Mohseni et al., 2012) and DBS-fMRI (Saenger et al., 2017a).

There is a long history of trying to characterize the global dynamics of brain activity in terms of complexity and dynamical stability, particularly in EEG studies (Pereda et al., 1998; Stam, 2005). The general picture that emerges is that brain activity during some diseases, coma and sleep is characterised by dynamical stability and loss of complexity. This phenomenon has been variously characterised in terms of principal component analysis and related decompositions into spatial modes, correlation dimension and dynamical formulations in terms of Lyapunov exponents (Pradhan and Sadasivan, 1996). Indeed, the (fractal) dimension is usually estimated using the Kaplan-Yorke conjecture, based upon estimates of Lyapunov exponents. Heuristically, the Lyapunov exponents reflect the degree of dissipation, decay or relaxation rate of various modes following endogenous or exogenous perturbation (Pradhan and Sadasivan, 1996). In sleep and some pathological brain states the fall in complexity of brain activity is generally accompanied by a loss of critical unstable modes, which increases dynamical stability usually associated with the emergence of slow brain rhythms.

Using an artificial perturbative approach, Massimini and colleagues investigated the perturbation-elicited changes in global brain activity during wakefulness and sleep using TMS-EEG, showing that non-REM sleep is accompanied by a breakdown in cortical effective connectivity, where the stimuli rapidly extinguish and do not propagate beyond the stimulation site (Massimini et al., 2005; Ferrarelli et al., 2010; Casali et al., 2013). These findings corroborate leading theories of consciousness postulating that consciousness requires effective communication between brain regions (Dehaene et al., 1998, 2014; Tononi et al., 1998; Dehaene et al., 2014), which appears impaired in certain stages of sleep and anesthesia (Alkire et al., 2008).

To assess the brain-wide spatiotemporal propagation of external stimulation Casali et al. (2013) introduced the Perturbational Complexity Index (PCI), which measures the amount of information contained in the amplitude of the average perturbation-elicited responses by calculating the Lempel-Ziv complexity of the binary matrix describing the statistically significant sources, in space and time, of the EEG signals,. PCI has been successfully used for separation of brain states in healthy subjects during wakefulness, dreaming, sleep, under different levels of anesthesia and in coma (Ferrarelli et al., 2010; Rosanova et al., 2012; Casali et al., 2013). Nevertheless, it is important to note that PCI is obtained from a grand average of an evoked potential, typically with relatively short latencies of 1–2 s, and ignores the pre-existing variability prior to every individual perturbation as well as the variability in responses across the series of perturbations.

In this paper, we expand to a new level the traditional perturbative approaches by using a whole-brain computational model that can be systematically perturbed off-line *in silico* in ways not possible *in vivo*. This allows for a deeper investigation of the biophysical mechanisms underlying the changes in dynamical complexity observed experimentally between brain states. We use a previously-published whole-brain model that directly models the network dynamics occurring at the ultra-slow scale of resting-state BOLD signal fluctuations without explicitly having to model the hemodynamic response function (Ponce-Alvarez et al., 2015; Deco et al., 2017b; Jobst et al., 2017; Saenger et al., 2017a). Using this approach, in Jobst et al. (2017) we have recently shown that fMRI dynamics of wakefulness and deep sleep can be differentiated by a global coupling parameter that shifts the dynamical regime of the network model.

Following these recent theoretical and experimental insights, we hypothesize that the *in silico* perturbation of the sleep model would result in a faster rate of decay of prominent synchronization modes relative to the awake model, consistent with less complex and more stable dynamics. Operationally, we conjecture that this is associated with a shift in the brain's dynamical regime, which alters the rate of dissipation of induced (or disrupted) synchronization among coupled brain areas, perhaps linked to the phenomenon of critical slowing down (Wissel, 1984; Van Nes and Scheffer, 2007). We measure this dissipation using the Perturbative Integration Latency Index (PILI), which measures the *recovery* of global integration levels back to baseline, scoring the persistence of the largest connected component in terms of BOLD phase synchronization.

Methods

Overview of perturbative approach

The following procedure, illustrated in Fig. 1, was implemented:

1. Fit the whole-brain computational model to fMRI data recorded in each brain state, i.e. during wakefulness and deep sleep (stage N3).
2. Compute from simulations the evolution of integration for each unperturbed brain state.
3. Systematic application of two off-line perturbation protocols (noise and synchronization) in 1–10 random brain regions and compute the evolution of integration after the offset of perturbation for each brain state.
4. Compute the PILI as the area under the normalized curve of perturbed integration until it reaches the basal integration levels. Repeat trials to estimate significance levels.

Experimental data

We used fMRI data from two independent studies recorded in Frankfurt, Germany (Tagliazucchi and Laufs, 2014) and Liège, Belgium (Boly et al., 2012) where participants fell asleep during a simultaneous EEG-fMRI scanning session. Both datasets have been described in previous publications and we only provide a brief summary of their acquisition and pre-processing here (see Supplementary Methods for more details). For this study, we only considered the subset of subjects who reached deep sleep (stage N3).

Frankfurt dataset: From a total of fifty-five subjects (thirty-six females, mean ± SD age of 23.4 ± 3.3 years) who fell asleep during a simultaneous EEG-fMRI recording previously described in Tagliazucchi and Laufs (2014), we selected the 18 subjects who reached stage N3 sleep (deep

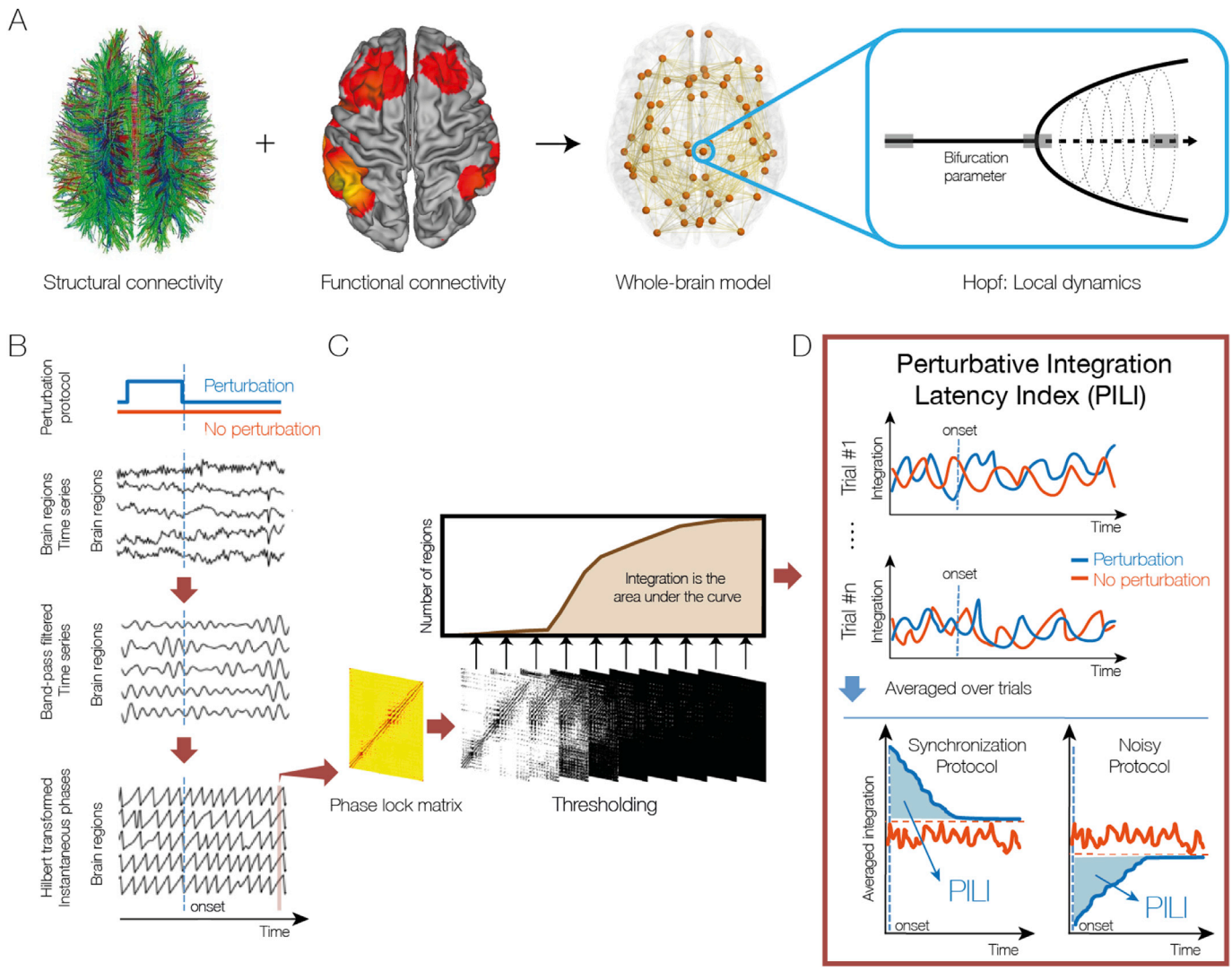

Fig. 1. Procedure for computing the Perturbative Integration Latency Index (PILI). A) First, the whole-brain computational model is constructed based on the empirical structural and functional connectivity between 90 brain regions, each represented by a Hopf bifurcation model. B) Second, the simulated time series for each brain region are band-pass filtered and the instantaneous phases obtained using the Hilbert transform. C) Third, the integration is calculated over 200 s in the basal unperturbed state and after the suppression of a perturbation protocol. For each time point a phase locking matrix is constructed and binarized, calculating the number of regions in the largest connected component for each threshold value. The integration is defined as the integral over all thresholds. D) Finally, the PILI is computed to characterize, in a single value, the recovery to basal equilibrium after the suppression of perturbation. PILI is computed as the integral between the curves of integration values over time (in light blue) for the perturbed dynamics (dark blue line) compared to the maximum or minimum (red dotted line) of the basal state dynamics (red line) (see *Methods* for details).

sleep). The mean duration (±standard deviation) of contiguous N3 sleep epochs for these participants was 11.67 ± 8.66 min fMRI data was recorded at 3T (Siemens Trio, Erlangen, Germany) simultaneously with EEG data using an MR-compatible EEG cap (modified BrainCapMR, Easycap, Herrsching, Germany). Sleep stages were scored manually by an expert according to the AASM criteria (AASM, 2007). fMRI data was realigned, normalized and spatially smoothed using SPM8 (www.fil.ion.ucl.ac.uk/spm). Cardiac, respiratory, and motion-induced noise were regressed out from the fMRI BOLD signals (Glover et al., 2000) and data was band-pass filtered in the range 0.01–0.1 Hz (Cordes et al., 2001). Please see the Supplementary Methods and Tagliazucchi and Laufs (2014) for full acquisition, pre-processing and sleep scoring details.

Liège dataset: We selected only the 12 participants who maintained sustained periods of wakefulness and deep NREM sleep (stage N3) from a dataset of twenty-five healthy young adults who underwent an EEG-fMRI session (eleven females, mean age of 22.0 years; age range 18–25 years) as described in a previous study by Boly et al. (2012). EEG data was acquired simultaneously with fMRI data to identify periods of wakefulness and 2–4 NREM sleep stages using an MR-compatible EEG cap (Braincap MR; Falk Minow Services) with 64 ring-type electrodes and two MR-compatible 32-channel amplifiers (Brainamp MR plus; Brain Products) in a 3-Tesla MR scanner (Allegra; Siemens). Pre-processing of the fMRI data was carried out using MELODIC 3.14 (Beckmann and Smith, 2004), part of FSL (FMRIB's Software Library, www.fmrib.ox.ac.uk/fsl). Please see the Supplementary Methods and Boly et al. (2012) for full acquisition, pre-processing and sleep scoring details.

fMRI processing

For each participant and for each brain state (i.e. wakefulness and deep sleep), we used FSL tools to normalize, extract and average the BOLD signals from all voxels within each ROI defined in the AAL atlas (considering only the 90 cortical and subcortical non-cerebellar brain regions) (Tzourio-Mazoyer et al., 2002) (see Supplementary Methods for full description).

Pairwise Pearson correlation between all 90 regions was computed resulting in a 90 × 90 functional connectivity (FC) matrix for each participant and brain state. Correlation values were converted to z-values applying Fisher's transform before averaging across participants in the

same cohort, resulting in a 90 × 90 FC matrix for each brain state (rest and sleep) and for each dataset (Frankfurt and Liège).

Structural connectivity

In the whole-brain network model, the interactions between the 90 brain areas were scaled in proportion to their white matter structural connectivity (Fig. 1A). For the present study, we used the structural connectivity between the 90 AAL regions obtained in a previous study (Deco et al., 2017a) averaged across 16 healthy young adults (5 females, mean ± SD age: 24.75 ± 2.54). Briefly, for each subject, a 90 × 90 structural connectivity matrix C was obtained by applying tractography algorithms to Diffusion Tensor Imaging (DTI) following the same methodology described in Cabral et al. (2012b) where the connectivity C_{np} between regions n and p is calculated as the proportion of sampled fibres in all voxels in region n that reach any voxel in region p. Since DTI does not capture fiber directionality, C_{np} was defined as the average between C_{np} and C_{pn}. Averaging across all 16 participants resulted in a structural connectivity matrix C representative of healthy young adults.

Whole-brain computational model

We simulated the BOLD activity at the whole-brain level using a phenomenological computational model, which emulates the ultra-slow resting-state dynamics captured by the BOLD signal by simulating the interactions between brain areas on this time scale when coupled through the anatomical structural connectivity (Kringelbach et al., 2015; Deco et al., 2017b). Notably, Jobst et al. (2017) have recently shown that the model parameters can be adjusted in order to describe different brain states such as wakefulness and deep sleep. The model consists of 90 coupled dynamical units (nodes) representing the 90 cortical and subcortical brain areas from the AAL parcellation explained above.

The BOLD activity of each brain area (node) is described by the normal form of a supercritical Hopf bifurcation (see Fig. 1A), which is the canonical model for studying the transition from noisy to oscillatory dynamics (Kuznetsov, 1998), as in (Deco et al., 2017b; Jobst et al., 2017; Saenger et al., 2017a). When coupled together using brain network architectures, the complex interactions between Hopf oscillators have been shown to successfully replicate features of brain dynamics observed at different time-scales including electrophysiology (Freyer et al., 2011, 2012), magnetoencephalography (Deco et al., 2017a) and fMRI (Kringelbach et al., 2015; Deco et al., 2017b). Since we were interested here in modeling the slow BOLD signal fluctuations observed in the different brain states, we adjusted the intrinsic frequency $f_n=\omega_n/2\pi$ of each node n to the empirical peak frequency of the BOLD signal in each brain region and for each brain state, as in Deco et al. (2017b) within the frequency range 0.04–0.07 Hz which has been shown to be the most reliable and functionally relevant for studies of resting-state activity (Biswal et al., 1995; Achard et al., 2006; Buckner et al., 2009; Glerean et al., 2012). The distributions of peak frequencies are reported in Figs. S1 and S2 in the Supplementary Information.

The dynamics of an uncoupled node n is given by the following set of coupled dynamical equations, which describes the normal form of a supercritical Hopf bifurcation in Cartesian coordinates:

$$\frac{dx_n}{dt} = \left[a_n - x_n^2 - y_n^2\right]x_n - \omega_n y_n + \beta\eta_n(t) \quad (1)$$

$$\frac{dy_n}{dt} = \left[a_n - x_n^2 - y_n^2\right]y_n + \omega_n x_n + \beta\eta_n(t) \quad (2)$$

where $\eta_n(t)$ is additive Gaussian noise with standard deviation β. This normal form has a supercritical bifurcation at $a_n = 0$, so that if $a_n>0$ the system engages in a stable limit cycle with frequency $f_n=\omega_n/2\pi$ and for $a_n<0$ the local dynamics returns to a stable fixed point representing a low activity noisy state.

To model the whole-brain dynamics we added an additive coupling term representing the input received in node n from every other node p, which is weighted by the corresponding structural connectivity C_{np}. This input was modeled using the common difference coupling, which approximates the simplest (linear) part of a general coupling function. Thus, the whole-brain dynamics was defined by the following set of coupled equations:

$$\frac{dx_n}{dt} = \left[a_n - x_n^2 - y_n^2\right]x_n - \omega_n y_n + G\sum_{p=1}^{N} C_{np}\left(x_p - x_n\right) + \beta\eta_n(t) \quad (3)$$

$$\frac{dy_n}{dt} = \left[a_n - x_n^2 - y_n^2\right]y_n + \omega_n x_n + G\sum_{p=1}^{N} C_{np}\left(y_p - y_p\right) + \beta\eta_j(t) \quad (4)$$

where G denotes the global coupling weight, scaling equally the total input received in each brain area. We fixed the noise standard deviation to $\beta = 0.02$ and the mean structural connectivity to <C>=0.2, in order to be in the same range of parameters previously explored in Deco et al. (2017b) and Jobst et al. (2017).

While the oscillators are weakly coupled, the periodic orbit of the uncoupled oscillators is preserved. Please note that we do not address here the case of non-linear coupling, in which the next non-vanishing higher order term following a Taylor expansion of the full coupling should be considered (Kuramoto, 1984; Pikovsky et al., 2003).

Due to the mesoscopic nature of the ultra-slow Hopf model considered herein - which explicitly neglects the contribution of faster neurophysiological rhythms - the variable x_n directly emulates the ultra-slow dynamics of the BOLD signal at each node n, without the need to apply an hemodynamic response function, which is necessary in more detailed models of neuronal activity (see also Cabral et al. (2017) for a review exposing this difference between neuronal and mesoscopic models). The global coupling parameter G is the control parameter with which we adjusted the model to the dynamical working region where the simulations optimally fit the empirical data (Deco et al., 2017b; Jobst et al., 2017).

Fitting the model to empirical data

To obtain a representative model of BOLD activity in both wakefulness and deep sleep, we first adjusted the model parameters to fit the spatio-temporal dynamics of BOLD signals recorded in each brain state and in each dataset.

In order to mimic the unperturbed basal dynamics in wakefulness and deep sleep, we followed the study by Jobst et al. (2017) who performed a careful exploration of the model's parameter space in terms of the global coupling G and the bifurcation parameter a in these two brain states. In particular, they have found that the optimal fit was obtained when the nodes operate in the vicinity of the bifurcation ($-0.1 \leq a \leq 0$) and, for a fixed a in this range, consistently occurred for higher G during wakefulness as compared to sleep (Jobst et al., 2017). As such, we fixed the local bifurcation parameters at $a_n = 0$ for all nodes, i.e. at the edge of a Hopf bifurcation describing the transition from a noisy to an oscillatory state as in Deco et al. (2017b), and adjusted only the global coupling parameter G in order to match the global level of BOLD phase synchronization measured empirically in each brain state, the most sensitive measure to distinguish the two brain states found in Jobst et al. (2017).

To match the level of BOLD phase synchronization, the BOLD signals (both empirical and simulated) were band-pass filtered within the narrowband 0.04–0.07 Hz and the time-varying phases $\varphi_n(t)$ of each narrowband signal were computed using the Hilbert transform (Fig. 1B) (Glerean et al., 2012; Ponce-Alvarez et al., 2015). The Hilbert transform represents a signal, $s(t)$, in the time domain as a rotating vector with an instantaneous phase, $\varphi(t)$, and an instantaneous amplitude, $A(t)$, as $s(t) = A(t)\cos(\varphi(t))$. Knowing the instantaneous phase $\varphi_i(t)$ of each narrowband BOLD signal at node n, the level of global BOLD phase synchronization over time is given by the Kuramoto order parameter (Kuramoto, 1984):

$$R(t) = \left| \sum_{n=1}^{N} e^{i\varphi_n(t)} \right| \Big/ N \quad (5)$$

where i is the imaginary unit and N is the total number of brain areas. If BOLD signals are completely independent, the N phases are uniformly distributed and R is nearly zero, whereas if the BOLD signals are fully synchronized, all phases are equal and $R = 1$. For each value of G ranging between 0 and 1 (with increments of 0.01), we compute the absolute difference between the mean levels of synchronization of simulated and empirical BOLD signals for each brain state and each dataset (see Fig. 2, red lines). Note that, for the mean levels of BOLD phase synchronization to be meaningful, the global signal should not be regressed out.

In addition, for each value of G, we calculated a simulated FC matrix as the 90 × 90 correlation matrix between the simulated BOLD signals (x_n) in all 90 regions. Correlation values were converted to z-values applying Fisher's transform and the simulated FC matrices were compared to the empirical ones obtained for each brain state (see *Methods - fMRI processing*) by calculating the Pearson correlation coefficient between the elements of the upper triangular part of both empirical and simulated FC matrices.

Off-line perturbation protocols

Despite being purely phenomenological, the Hopf model is particularly well-suited for perturbative studies because each brain area n has a local parameter a_n that defines the distance to a supercritical Hopf bifurcation, inducing synchronized BOLD fluctuations for $a_n>0$ and strong noise for $a_n<0$ (Kringelbach et al., 2015; Deco et al., 2017b). We used two different off-line perturbation protocols eliciting strong deviations from the basal (i.e. unperturbed) state dynamics by artificially imposing more synchronization or temporarily suppressing synchronization in different brain regions. In order to attenuate the local effects associated to the perturbation of specific brain areas, we systematically repeated each protocol 3000 times, perturbing a different set of randomly selected brain regions in each trial.

1) *Synchronization perturbation protocol*: 1 to 10 randomly selected brain regions were simultaneously perturbed for 100 s by shifting their local bifurcation parameter values to the positive range ($a_n = 0.6$), which imposes more synchronized oscillatory BOLD signals.
2) *Noise perturbation protocol:* To temporarily suppress synchronization, the local parameters of 1–10 randomly selected brain regions were simultaneously shifted to the negative region ($a_i = -0.6$) for 100 s eliciting more noisy behaviour and hence causing an artificial perturbative destruction of the basal synchronization across the different brain areas.

In both protocols, the bifurcation parameters were reset to zero after perturbation.

Integration over time

To characterize the level of brain-wide BOLD signal interactions across time, we used an observable measure that summarizes in a single value for each time point the level of *Integration* across the whole brain previously defined in Deco et al. (2015), and which characterizes the broadness of communication between brain regions at the instantaneous level (Lord et al., 2017).

To calculate the Integration, first we use the BOLD signal phases $\varphi_n(t)$ (obtained using the Hilbert transform, see *Methods - Fitting simulations to empirical data*) to calculate a *phase locking matrix P,* describing for each time point the level of pair-wise phase synchronization between regions n and p as:

$$P_{np}(t) = \mathrm{Re}\left| e^{-3(\varphi_n(t)-\varphi_p(t))} \right| = \cos\left(\varphi_n(t) - \varphi_p(t)\right) \quad (6)$$

Based on this phase locking matrix, we compute the level of integration $I(t)$ at each time point t as the size of the largest connected component of $P(t)$ averaged over thresholds (Deco et al., 2015). More specifically, for a given absolute threshold θ between 0 and 1 (scanning the whole range), P is binarized (0, if $|P_{np}| < \theta$, θ and 1 otherwise). For each threshold θ and for each time t, the number of nodes in the largest

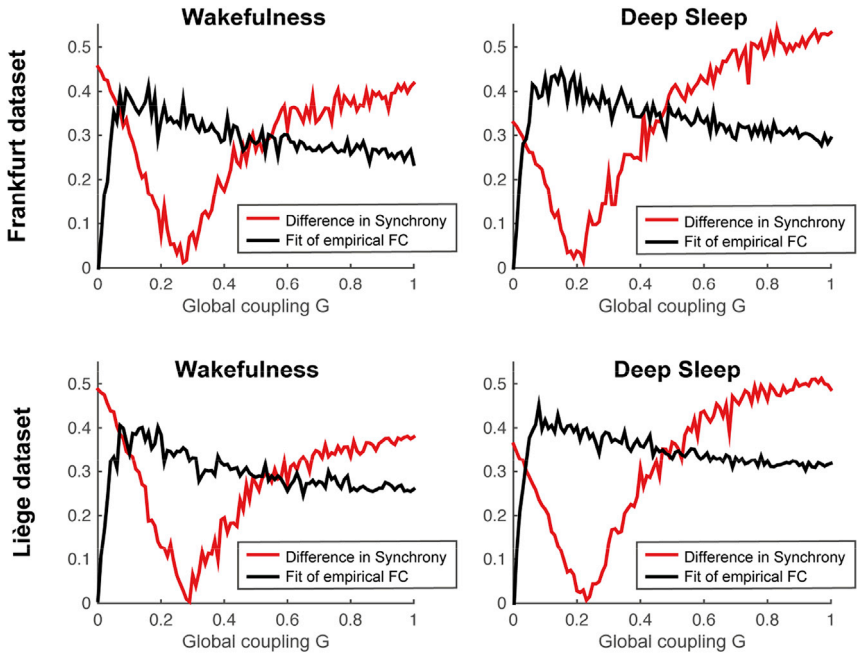

Fig. 2. Adjusting the whole-brain Hopf model to the basal brain activity of wakefulness and deep sleep. Before applying the perturbative protocol, we first define the model parameters of the whole-brain Hopf model in order to obtain a representative model of the brain activity recorded during wakeful rest and deep sleep using fMRI from two independent studies (Frankfurt and Liège) (Jobst et al., 2017). The red line shows the difference between synchrony degrees, such that, when the synchrony error reaches zero, the mean synchrony degree of simulated BOLD signals matches the one measured empirically. In addition, the black line shows the correlation between empirical and simulated FC matrices, which is kept high for the range where the synchronization error is optimal.

connected component of $P(t)$ is extracted (see Fig. 1C). The largest component is the largest sub-graph of the binarized $P(t)$, in which any two vertices are connected to each other by paths, and which connects to no additional vertices. In order to be independent of a given threshold, we repeat this procedure scanning all possible thresholds (between 0 and 1) and define the Integration at each time t, $I(t)$, as the integral of the largest component curve as a function of the thresholds. We have recently shown that this measure is both sensitive and specific with the ability to classify FC differences associated with different diseases and brain states (Deco et al., 2015). Following this procedure, we calculated the Integration over 200 s of simulated BOLD signals in the basal conditions and right after perturbation offset.

Perturbative Integration Latency Index

The Perturbative Integration Latency Index (PILI) characterizes the recovery of the perturbed brain dynamics to regain basal equilibrium after suppression of the perturbation (see Fig. 1D). The key idea is to characterize the latency of extinction of a massive stimulation perturbing a basal state. Thus, to determine when the evoked perturbative dynamics relaxes back to the basal dynamics of wakefulness or deep sleep after the offset of perturbation, we measure the alterations in the level of integration over time (see Fig. 1D).

In more detail, we first compute the Integration for 200 s of the simulated unperturbed basal cases, and detect the maximal and minimal values, I_{max}^{basal} and I_{min}^{basal}, for each brain state (see Fig. 3, red lines). Then, we perturb the system and compute the integration for 200 s after the offset of perturbation, averaged across 3000 trials. The values I_{max}^{basal} and I_{min}^{basal} are used as the criterion for reaching the basal values for the synchronization and for the noisy perturbative protocols, respectively. The PILI is obtained by normalizing the extrema of I to 1 at the offset of perturbation (i.e. for $t = 0$) and 0 at the point where the Integration reaches the basal values and calculating the integral of that curve. Larger values of this integral mean longer latency of extinction of the perturbative effects and smaller values indicate shorter latencies. The process is sketched in Fig. 1. Significance levels were estimated over 3000 trials, calculating the mean of the distribution and estimating the error.

Node-wise perturbations

To explore the link between localized PILI and other node-wise metrics, we computed PILI after 1000 synchronous and noisy perturbations one node at a time. We then correlated the resulting mean PILI vectors (shown in Fig. 5A) with different metrics characterizing the critical dynamics and the functional and structural connectivity strengths (shown in Fig. 5B). The first index was used to explore the relationship between PILI and critical dynamics by taking into account the bifurcation parameters (a_n in equations (3) and (4)) optimized at each node n (Deco et al., 2017b; Jobst et al., 2017). Importantly, the resulting regional PILI values are also computed by taking into account the optimized bifurcation parameter distribution, so in this part of the analysis, the values of the bifurcation parameter across nodes are not set to ~0 but rather to their expected values. This constrains the localized perturbations with the "true" underlying critical dynamics allowing a closer linkage with topology. Secondly, we used the strength (sum of connectivity weights per node) of the mean FC matrix for both sleep and awake states. This allowed uncovering a possible relation between PILI and the underlying functional connectivity. Finally, we used the strength of the structural connectivity (obtained from the SC matrix) to explore the relation between structural properties of brain connectivity and PILI. All correlations were corrected for multiple comparisons. Only those correlations with $p < 0.008$ were considered as significant.

Results

We investigated the differences between two brain states, wakefulness and deep sleep, in healthy human participants from 2 independent previously published studies using a new off-line perturbative approach

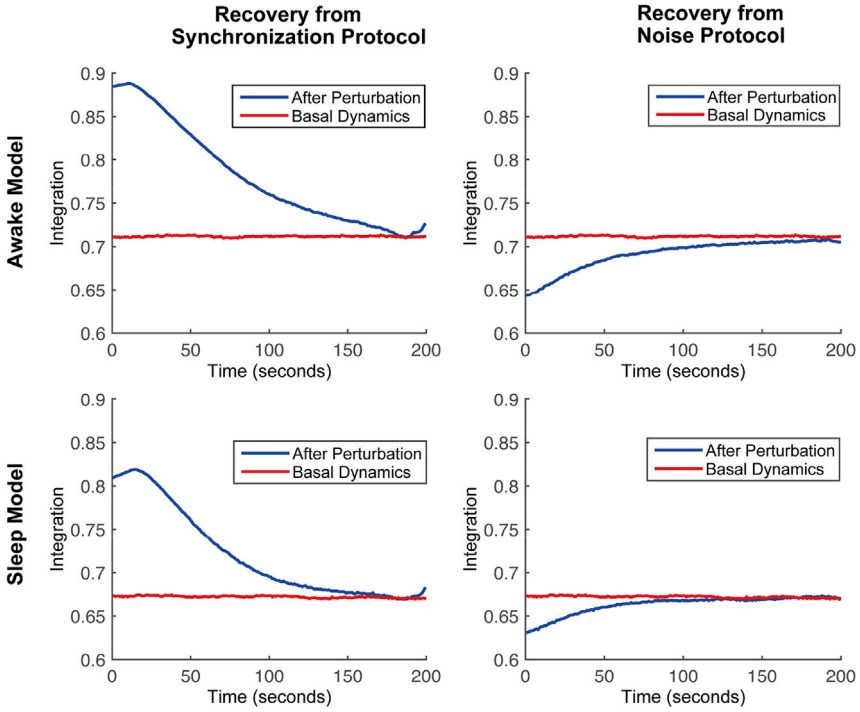

Fig. 3. Response to perturbation *in silico* for wakefulness and deep sleep. (Blue lines) Responses in the level of global integration after 10 random brain areas were perturbed using the synchronization protocol (left column) or the noise protocol (right column) during wakefulness (top line) and deep sleep (bottom line) averaged over 3000 trials. (Red lines) Baseline levels of integration in the unperturbed simulated dynamics, different for wakefulness (top) and deep sleep (bottom). Once perturbation is halted (at $t = 0$s), the integration slowly decays (left) or rises (right) towards the baseline values of each state (see *Methods* for details). For the purpose of illustration, the results are shown for the Frankfurt dataset only, but similar plots were obtained with the Liège dataset.

in which we focused on the latency that the system takes to recover back to baseline after the offset of a strong multifocal perturbation applied off-line (the methods are summarized in Fig. 1).

As a first step, the whole-brain computational model was adjusted to the baseline activity of each brain state recorded with fMRI in each study (see *Methods - Fitting the model to empirical data*). In Fig. 2 (red lines) we show how the global coupling parameter G was adjusted such that the mean degree of synchronization in simulated BOLD signals matched the ones measured empirically in each brain state and in each dataset. We found that this match – i.e. when the difference between the mean synchronization levels reaches zero (red lines) – occurs for a very specific value of G, which is consistently lower in deep sleep than wakefulness for both datasets. This result goes in agreement with previous findings suggesting that functional connectivity at the level of the BOLD signals is stronger during wakefulness than deep sleep (Jobst et al., 2017). In addition, we show in Fig. 2 (black lines) the correlation between the empirical and simulated FC matrices as a function of G. This measure, however, is less constrictive since a good fit is obtained not only for the optimal G determined above but also when the simulated BOLD signals highly differed from the real ones in terms of phase synchronization.

Once we obtained a representative model of the whole-brain dynamics of each brain state, i.e. a Wakefulness Model and a Sleep Model (adjusted to each dataset), the models were perturbed off-line following two distinct perturbation protocols in which we induced either more synchronization or more noise in 1–10 random brain regions for 100 s (see *Methods - Off-line perturbation protocols*). After perturbation was stopped, we measured the perturbation-elicited changes in terms of global Integration, which captures the brain-wide connectedness of BOLD signals in terms of phase locking (see *Methods – Integration over time*) (Deco et al., 2015; Lord et al., 2017).

In Fig. 3, we show the evolution of Integration (averaged over 3000 trials) right after the perturbation of 10 random brain areas (blue lines) compared to the basal condition (red lines) for each model and for each perturbation protocol. Notably, the basal Integration was consistently higher during wakefulness (red line, top plots) than during sleep (red line, bottom plots), which means a higher connectedness at the level of BOLD signal phases during unperturbed wakefulness. At the offset of a long-lasting perturbation, i.e. at t = 0 (blue lines), the levels of Integration are strongly deviated from the baseline, with increased Integration after the synchronization protocol (left plots) and decreased Integration after the noise protocol (right plots). During the recovery period, the levels of integration slowly decay (or rise) towards their corresponding basal levels lasting on average more than 100 s to fully recover. Importantly, we found that each brain state, here wakefulness and sleep, recovered differently after being submitted to the same perturbation protocols.

To characterize the recovery after a long-lasting perturbation, we defined the Perturbative Integration Latency Index (PILI), which can be interpreted from Fig. 3 as the area between the normalized red and blue curves. To capture only the recovery dynamics in the PILI, the curves of perturbed integration are normalized such that $I(t_0)=1$ at the offset of perturbation, irrespective of the brain state, and $I=0$ at the point where the Integration reaches the basal values. We calculated the PILI for each brain state and each perturbation protocol with varying number of perturbed areas. In Fig. 4, we show the values of PILI as a function of the number of brain regions perturbed, for each brain state and synchronization protocol. Importantly, for both datasets, we found consistently higher PILI for wakefulness than for sleep, with significance $p < 10^{-5}$, irrespective of the number of nodes perturbed. This result shows that two brain states, here wakefulness and deep sleep, can be dissociated based on their dynamical response to a strong long-lasting perturbation, which is efficiently characterised using PILI. Whether the perturbation acts on promoting or disrupting synchronization, the recovery is consistently longer during wakefulness than in deep sleep.

Finally, we studied the effects of perturbation on a node-by-node level by computing the corresponding PILI profiles after both noisy and synchronous perturbation in the sleep and awake brain (Fig. 5A). Because a crucial point is to explore how this metric relates with the underlying topology of each node, we explored the relationship between the resulting PILI profiles and other nodal metrics. We first explored the correlation between PILI profiles and the optimized critical dynamics of each brain area by considering the optimized bifurcation parameters as in Deco et al. (2017b). This correlation yielded high significant values for both sleep ($r = 0.54$, $p < 0.0001$) and wakefulness ($r = 0.83$, $p < 0.0001$) after noisy but not for synchronous perturbation (Fig. 5C, top). To explore a possible link of localized PILI with a simpler topological metric, we used the Strength (sum of region-specific weights) of both structural and functional matrices, which conveniently is not sensitive to arbitrary thresholding (Saenger et al., 2017b). Here, PILI values after noisy perturbation significantly correlated with structural strength in both sleep ($r = 0.34$, $p < 0.0001$) and awake ($r = 0.52$, $p < 0.0001$). The only other correlation that survived correction for multiple comparisons was that between PILI after noisy perturbation and functional strength in the awake brain ($r = 0.51$, $p < 0.0001$).

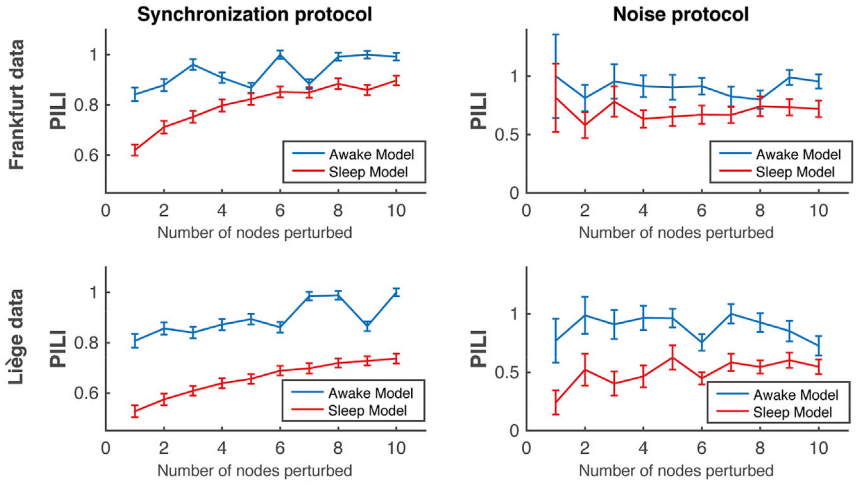

Fig. 4. Slower recoveries in the Awake model compared to the Sleep model following systematic perturbation reveal critical slowing down of the network dynamics. Mean PILI values obtained in the awake (blue) and deep sleep (red) models as a function of the number of random brain regions perturbed, for each dataset and perturbation protocol. Larger PILI values correspond to slower recovery rate. Errorbars represent the standard error of the mean over 3000 trials. We found clear significant differences in PILI between wakefulness and deep sleep, with p-value$<10^{-5}$, in both datasets and synchronization protocols.

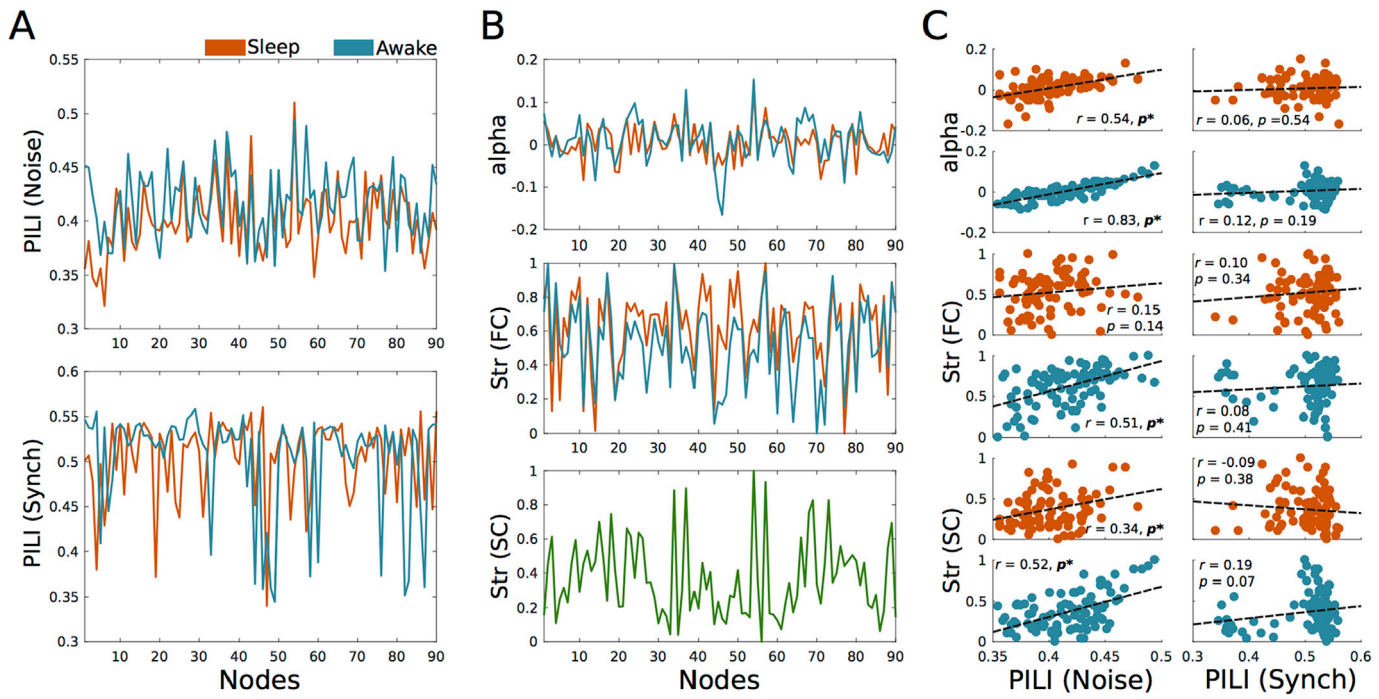

Fig. 5. Node-wise changes after noisy and synchronous perturbation in the sleep (red) and awake (blue) brain models. A) Mean Perturbative Integration Latency Index (PILI) after 1000 perturbation to each of the N = 90 nodes using the Noise (top) or the Synchronization (bottom) perturbation protocols. B) Three node-wise metrics used for the comparisons in panel C: The bifurcation parameter (alpha or a in the model equations) optimized for each node following the approach from Deco et al. (2017b) (top), the mean functional connectivity strength Str(FC) of each node (middle) and the mean structural connectivity strength Str(SC) of each node (bottom). C) Correlation scatters between PILI and all the node-wise metrics from panel B. p^* represents a $p < 0.0001$, which reflects significance after correcting for multiple comparisons.

Discussion

In this paper we introduced a novel methodological approach designed to investigate the dynamical complexity of brain states through their recovery from strong long-lasting perturbations using PILI. This approach has the potential to significantly expand our understanding of the dynamical complexity underlying different conscious and unconscious states. Our results show that PILI efficiently dissociated two brain states, here wakefulness and deep sleep, with significantly higher PILI in wakefulness in both datasets and perturbation protocols, regardless of the number of areas perturbed. Overall, these results show that a shift in the dynamical regime of the brain – induced by a change in the global coupling weight potentially linked to cholinergic levels (Deco et al., 2014) – turns the brain more rigid to external perturbations during deep sleep, returning faster to its equilibrium dynamics, whereas during wakefulness the brain integrates perturbations in the dynamics for longer. Theoretically, these results express the critical slowing down of a system when it is shifted away from an equilibrium point (Wissel, 1984; Van Nes and Scheffer, 2007), in line with previous EEG studies showing that sleep is characterised by dynamical stability and loss of complexity (Pereda et al., 1998).

Importantly, all perturbations in this work are applied off-line to a whole-brain computational model, which allows eliciting strong unnatural deviations from the basal activity with recoveries lasting more than a hundred seconds. The model is previously adjusted to the basal activity recorded with fMRI in each brain state, here wakefulness and deep sleep, resulting in two distinct models representative of each unperturbed brain state (Jobst et al., 2017). These models can then be exhaustively perturbed *in silico* without the ethical and safety constrains of *in vivo* perturbations (Clausen, 2010; Kringelbach and Aziz, 2011). Previous studies have used whole-brain computational models to simulate the effects of structural lesions, i.e. by removing links or nodes, and studying its impact in whole-brain dynamics (Cabral et al., 2012a; Vasa et al., 2015; Aerts et al., 2016; Deco et al., 2017c). In particular, we have recently shown that the removal of specific 'binding' regions impacts subsequent brain activity, specifically in terms of integration and information encoding capability (Deco et al., 2017c). Rather than removing regions, we perturbed regions by making them either more oscillatory or more noisy and measured the recovery of the system's global integration. Other studies have recently started to locally perturb models of resting-state activity to investigate their response to stimulation, particularly focusing on the activation/stabilization of meaningful functional networks in task (Cocchi et al., 2015; Gollo et al., 2016; Spiegler et al., 2016). Yet the strategy presented herein differs from previous off-line stimulation approaches because it does not aim to simulate natural perturbative interventions (pathological or not) but rather to further investigate why brain states can be dissociated based on their response to perturbations, revealing important features of their dynamical complexity.

In terms of the elicited changes resulting from the perturbation of individual nodes, we found positive and significant correlations between the elicited PILI and other metrics characteristic of each brain area. Interestingly, the highest and most significant correlations were observed between the resulting PILI and the optimized bifurcation parameters, which suggest a closer relationship between PILI and the critical dynamics of each brain area rather than with static or topological features. Relevant to this argument, it has been recently shown that the most relevant hubs in the brain within a functional perspective are not necessarily those extracted after taking into account static structural features such a rich-club ranking (Deco et al., 2017b). This observation suggests that, although structure and function are closely related, the intrinsic node dynamics also plays a fundamental role in promoting the relevance of such regions. Also worth noting is that overall, correlations were higher in the awake brain, which suggests that the link between PILI and functional/structural metrics is tightened while awake, and diminished during sleep. Further studies exploring this relation in more detail would be of considerable interest.

The introduction of our novel method for revealing the dynamical complexity following systematic perturbation is complementary to the seminal work of Massimini and colleagues who have used TMS with EEG for characterizing different conscious brain states (e.g. wakefulness, sleep

and anesthesia) (Massimini et al., 2005; Ferrarelli et al., 2010; Casali et al., 2013). In contrast to this previous method, which uses brief TMS pulses and thus measures the weak perturbation-elicited dynamics, our approach measures the *recovery* after the offset of a long-lasting perturbation. Moreover, since the perturbation-evoked activity is influenced by fluctuations in spontaneous brain activity present at the time of perturbation, we reduce the effect of such fluctuations by strongly deviating the dynamics from the basal activity through a substantial long-lasting perturbation – only possible in a computational model - and then measuring the recovery from this perturbation over 3000 trials.

Following a growing trend in the analysis of dynamic BOLD signal connectivity, we consider only the coupling at the level of BOLD phases (Glerean et al., 2012; Cabral et al., 2017; Deco et al., 2017a). Measuring changes in phase space allows for a better characterization of the rich BOLD signal dynamics and any changes arising from perturbations. In particular, this makes it possible to directly determine the global level of synchronization across the whole brain, to obtain the phase locking matrices at the instantaneous level and derive the global level of integration over time (Deco et al., 2015). This reduction to phase space relies on the fact that the non-linear brain dynamics shares more features with the non-linear phenomena observed in the waves and turbulence of the ocean than with that of a sedate pond, which can be characterised solely with amplitude measurements. The fundamental idea behind our hypothesis is that a strong perturbation to the turbulent “ocean” of brain activity elicits alterations in phase (rather than amplitude) space.

There are a number of limitations to our analysis that deserve mention. First, we have modeled directly the haemodynamics with a Hopf normal form model, which presupposes that the temporal scale of haemodynamics can be represented solely by the slow fluctuations of neuronal activity inherent in fMRI timeseries. Second, we are characterising the stability (or complexity) of coupled dynamical units - not the neuronal dynamics generating brain signals. Practically, this means that we have shown that changing the global (symmetric) coupling parameter G of coupled Hopf units induces a shift in the dynamical regime of the model, which changes its global stability (i.e. complexity). The importance of this observation has been motivated by previous results showing that the global coupling required to emulate sleep and waking functional connectivity in empirical data also changes (Jobst et al., 2017).

But the link between the empirical and the simulated dynamics does not rest solely upon global coupling. It is equally important to consider the role of specific BOLD frequencies, as the ones within the most meaningful resting-state narrow-band. We found a wider distribution of BOLD frequencies during sleep, which, in a network model, allows for increased segregation and lower integration. As such, the lower BOLD integration levels in the baseline sleep model are likely to be a combination of both the weaker coupling strength and the wider frequency distribution obtained from empirical data. Here, we show that these two features of brain dynamics shift the models’ dynamical regimes into different levels of baseline integration, which may be directly or indirectly related to different states of consciousness. Yet, other ingredients and features certainly play a role in regulating the dynamical complexity of different brain states, namely the asymmetric, region-specific and context-sensitive coupling in real brains. Since our methodological approach is not exclusive to the Hopf model used herein, it will be interesting in future work to fit more realistic models of effective connectivity to empirical data and pursue a more detailed characterization along the lines above.

Here we expose two dynamical features inducing changes in the complexity of brain activity while the underlying network structure remains intact, namely the global coupling strength and the intrinsic ultra-slow frequency of each brain area. From an analytic perspective, recent studies on the stability and controllability of the human brain's structural connectivity matrix have made significant achievements in relating the dynamical complexity with the underlying network architecture (Gu et al., 2015; Betzel et al., 2016), in particular under artificial stimulation (Muldoon et al., 2016). Overall, such analytical studies in combination with the insights obtained from numerical simulations have the potential to become important tools for the development of personalized stimulation protocols.

Overall, *in silico* perturbations of whole-brain dynamics open up for a new level of artificial perturbative studies unconstrained by ethical limitations allowing for a deeper investigation of the dynamical properties of different brain states. To introduce the model, we restricted our analysis to two healthy brain states, wakefulness and sleep, but it would be important to test the method on other natural or pathological brain states such as vegetative coma, minimal conscious state, locked-in syndrome and various levels of anesthesia (Casali et al., 2013; Deco and Kringelbach, 2014) or in altered states elicited by drugs such as morphine, amphetamines, psilocybin and LSD (Carhart-Harris et al., 2014).

Beyond the dissociation between brain states via massive perturbation protocols, the perturbative approach proposed herein offers a new strategy for effectively introducing probabilistic causality into neuroimaging studies and may be modified to further explore the minimal perturbation necessary to induce a significant dissociation between states, or to evaluate the efficacy of different perturbation protocols applied to different target regions. By offering the possibility to causally perturb a whole-brain computational model that fits human empirical neuroimaging data it could become a tool for determining where efficacious perturbation might help rebalance the dynamical complexity of the brain (Kringelbach et al., 2011; Saenger et al., 2017a). It may therefore be useful in clinical contexts for predicting the outcome of DBS or TMS for specific disorders, perhaps even at the individual level.

Conflict of interest

The authors declare to have no conflict of interest.

Acknowledgements

GD was supported by the ERC Advanced Grant: DYSTRUCTURE (n. 295129), by the Spanish Research Project SAF2010-16085 and the FP7-ICT BrainScales. MLK and JC were supported by the ERC Consolidator Grant: CAREGIVING (n. 615539) and Center for Music in the Brain, funded by the Danish National Research Foundation (DNRF117). JC was supported under the project NORTE-01-0145-FEDER-000023, supported by the Northern Portugal Regional Operational Programme (NORTE 2020), under the Portugal 2020 Partnership Agreement, through the European Regional Development Fund (FEDER).

Appendix A. Supplementary data

Supplementary data related to this article can be found at https://doi.org/10.1016/j.neuroimage.2017.12.009.

References

AASM, 2007. The AASM Manual for the Scoring of Sleep and Associated Events-rules. Terminology and Technical Specifications. American Academy of Sleep Medicine, Chicago.

Achard, S., Salvador, R., Whitcher, B., Suckling, J., Bullmore, E., 2006. A resilient, low-frequency, small-world human brain functional network with highly connected association cortical hubs. J. Neurosci. Off. J. Soc. Neurosci. 26, 63–72.

Aerts, H., Fias, W., Caeyenberghs, K., Marinazzo, D., 2016. Brain networks under attack: robustness properties and the impact of lesions. Brain A J. Neurol. 139, 3063–3083.

Alkire, M.T., Hudetz, A.G., Tononi, G., 2008. Consciousness and anesthesia. Science 322, 876–880.

Beckmann, C.F., Smith, S.M., 2004. Probabilistic independent component analysis for functional magnetic resonance imaging. IEEE Trans. Med. Imaging 23, 137–152.

Betzel, R.F., Gu, S., Medaglia, J.D., Pasqualetti, F., Bassett, D.S., 2016. Optimally controlling the human connectome: the role of network topology. Sci. Rep. 6, 30770.

Biswal, B., Yetkin, F., Haughton, V., Hyde, J., 1995. Functional connectivity in the motor cortex of resting human brain using echo-planar MRI. Magn. Reson. Med. Off. J. Soc. Magn. Reson. Med./Soc. Magn. Reson. Med. 34, 537–541.

Boly, M., Perlbarg, V., Marrelec, G., Schabus, M., Laureys, S., Doyon, J., Pelegrini-Issac, M., Maquet, P., Benali, H., 2012. Hierarchical clustering of brain activity during human nonrapid eye movement sleep. Proc. Natl. Acad. Sci. U. S. A. 109, 5856–5861.
Buckner, R.L., Sepulcre, J., Talukdar, T., Krienen, F.M., Liu, H., Hedden, T., Andrews-Hanna, J.R., Sperling, R.A., Johnson, K.A., 2009. Cortical hubs revealed by intrinsic functional connectivity: mapping, assessment of stability, and relation to Alzheimer's disease. J. Neurosci. Off. J. Soc. Neurosci. 29, 1860–1873.
Cabral, J., Hugues, E., Kringelbach, M.L., Deco, G., 2012a. Modeling the outcome of structural disconnection on resting-state functional connectivity. NeuroImage 62, 1342–1353.
Cabral, J., Kringelbach, M.L., Deco, G., 2012b. Functional graph alterations in schizophrenia: a result from a global anatomic decoupling? Pharmacopsychiatry 45 (Suppl. l), S57–S64.
Cabral, J., Kringelbach, M.L., Deco, G., 2014. Exploring the network dynamics underlying brain activity during rest. Prog. Neurobiol. 114, 102–131.
Cabral, J., Kringelbach, M.L., Deco, G., 2017. Functional connectivity dynamically evolves on multiple time-scales over a static structural connectome: models and mechanisms. Neuroimage 160, 84–96.
Carhart-Harris, R.L., Leech, R., Hellyer, P.J., Shanahan, M., Feilding, A., Tagliazucchi, E., Chialvo, D.R., Nutt, D., 2014. The entropic brain: a theory of conscious states informed by neuroimaging research with psychedelic drugs. Front. Hum. Neurosci. 8, 20.
Casali, A.G., Gosseries, O., Rosanova, M., Boly, M., Sarasso, S., Casali, K.R., Casarotto, S., Bruno, M.A., Laureys, S., Tononi, G., Massimini, M., 2013. A theoretically based index of consciousness independent of sensory processing and behavior. Sci. Transl. Med. 5, 198ra105.
Clausen, J., 2010. Ethical brain stimulation - neuroethics of deep brain stimulation in research and clinical practice. Eur. J. Neurosci. 32, 1152–1162.
Cocchi, L., Sale, M.V., Lord, A., Zalesky, A., Breakspear, M., Mattingley, J.B., 2015. Dissociable effects of local inhibitory and excitatory theta-burst stimulation on large-scale brain dynamics. J. Neurophysiol. 113, 3375–3385.
Cole, M.W., Bassett, D.S., Power, J.D., Braver, T.S., Petersen, S.E., 2014. Intrinsic and task-evoked network architectures of the human brain. Neuron 83, 238–251.
Cordes, D., Haughton, V.M., Arfanakis, K., Carew, J.D., Turski, P.A., Moritz, C.H., Quigley, M.A., Meyerand, M.E., 2001. Frequencies contributing to functional connectivity in the cerebral cortex in "resting-state" data. AJNR Am. J. Neuroradiol. 22, 1326–1333.
Damoiseaux, J.S., Rombouts, S.A., Barkhof, F., Scheltens, P., Stam, C.J., Smith, S.M., Beckmann, C.F., 2006. Consistent resting-state networks across healthy subjects. Proc. Natl. Acad. Sci. U. S. A. 103, 13848–13853.
Deco, G., Cabral, J., Woolrich, M.W., Stevner, A.B.A., van Hartevelt, T.J., Kringelbach, M.L., 2017a. Single or multiple frequency generators in on-going brain activity: a mechanistic whole-brain model of empirical MEG data. NeuroImage 152, 538–550.
Deco, G., Hagmann, P., Hudetz, A.G., Tononi, G., 2014. Modeling resting-state functional networks when the cortex falls asleep: local and global changes. Cereb. cortex 24, 3180–3194.
Deco, G., Jirsa, V.K., McIntosh, A.R., 2011. Emerging concepts for the dynamical organization of resting-state activity in the brain. Nat. Rev. Neurosci. 12, 43–56.
Deco, G., Kringelbach, M., 2016. Metastability and coherence: extending the communication through coherence hypothesis using a whole-brain computational perspective. Trends Neurosci. 39, 432.
Deco, G., Kringelbach, M.L., 2014. Great expectations: using whole-brain computational connectomics for understanding neuropsychiatric disorders. Neuron 84, 892–905.
Deco, G., Kringelbach, M.L., Jirsa, V.K., Ritter, P., 2017b. The dynamics of resting fluctuations in the brain: metastability and its dynamical cortical core. Sci. Rep. 7, 3095.
Deco, G., Tononi, G., Boly, M., Kringelbach, M.L., 2015. Rethinking segregation and integration: contributions of whole-brain modelling. Nat. Rev. Neurosci. 16, 430–439.
Deco, G., Van Hartevelt, T.J., Fernandes, H.M., Stevner, A., Kringelbach, M.L., 2017c. The most relevant human brain regions for functional connectivity: evidence for a dynamical workspace of binding nodes from whole-brain computational modelling. NeuroImage 146, 197–210.
Dehaene, S., Charles, L., King, J.R., Marti, S., 2014. Toward a computational theory of conscious processing. Curr. Opin. Neurobiol. 25, 76–84.
Dehaene, S., Kerszberg, M., Changeux, J.P., 1998. A neuronal model of a global workspace in effortful cognitive tasks. Proc. Natl. Acad. Sci. U. S. A. 95, 14529–14534.
Ferrarelli, F., Massimini, M., Sarasso, S., Casali, A., Riedner, B.A., Angelini, G., Tononi, G., Pearce, R.A., 2010. Breakdown in cortical effective connectivity during midazolam-induced loss of consciousness. Proc. Natl. Acad. Sci. U. S. A. 107, 2681–2686.
Fox, M.D., Buckner, R.L., Liu, H., Chakravarty, M.M., Lozano, A.M., Pascual-Leone, A., 2014. Resting-state networks link invasive and noninvasive brain stimulation across diverse psychiatric and neurological diseases. Proc. Natl. Acad. Sci. U. S. A. 111, E4367–E4375.
Freyer, F., Roberts, J.A., Becker, R., Robinson, P.A., Ritter, P., Breakspear, M., 2011. Biophysical mechanisms of multistability in resting-state cortical rhythms. J. Neurosci. Off. J. Soc. Neurosci. 31, 6353–6361.
Freyer, F., Roberts, J.A., Ritter, P., Breakspear, M., 2012. A canonical model of multistability and scale-invariance in biological systems. PLoS Comput. Biol. 8, e1002634.
Glerean, E., Salmi, J., Lahnakoski, J.M., Jaaskelainen, I.P., Sams, M., 2012. Functional magnetic resonance imaging phase synchronization as a measure of dynamic functional connectivity. Brain connect. 2, 91–101.
Glover, G.H., Li, T.Q., Ress, D., 2000. Image-based method for retrospective correction of physiological motion effects in fMRI: RETROICOR. Magn. Reson. Med. Off. J. Soc. Magn. Reson. Med./Soc. Magn. Reson. Med. 44, 162–167.
Gollo, L.L., Roberts, J., Cocchi, L., 2016. Mapping How Local Perturbations Influence Systems-level Brain Dynamics. Arxiv eprint arXiv:1609.00491.
Gu, S., Pasqualetti, F., Cieslak, M., Telesford, Q.K., Yu, A.B., Kahn, A.E., Medaglia, J.D., Vettel, J.M., Miller, M.B., Grafton, S.T., Bassett, D.S., 2015. Controllability of structural brain networks. Nat. Commun. 6, 8414.
Ilmoniemi, R.J., Virtanen, J., Ruohonen, J., Karhu, J., Aronen, H.J., Naatanen, R., Katila, T., 1997. Neuronal responses to magnetic stimulation reveal cortical reactivity and connectivity. Neuroreport 8, 3537–3540.
Jobst, B.M., Hindriks, R., Laufs, H., Tagliazucchi, E., Hahn, G., Ponce-Alvarez, A., Stevner, A.B.A., Kringelbach, M.L., Deco, G., 2017. Increased stability and breakdown of brain effective connectivity during slow-wave sleep: mechanistic insights from whole-brain computational modelling. Sci. Rep. 7, 4634.
Kringelbach, M.L., Aziz, T.Z., 2011. Neuroethical principles of deep brain stimulation. World Neurosurg. 76, 518–519.
Kringelbach, M.L., Green, A.L., Aziz, T.Z., 2011. Balancing the brain: resting state networks and deep brain stimulation. Front. Integr. Neurosci. 5, 8.
Kringelbach, M.L., Jenkinson, N., Green, A.L., Owen, S.L.F., Hansen, P.C., Cornelissen, P.L., Holliday, I.E., Stein, J., Aziz, T.Z., 2007a. Deep brain stimulation for chronic pain investigated with magnetoencephalography. Neuroreport 18, 223–228.
Kringelbach, M.L., Jenkinson, N., Owen, S.L.F., Aziz, T.Z., 2007b. Translational principles of deep brain stimulation. Nat. Rev. Neurosci. 8, 623–635.
Kringelbach, M.L., McIntosh, A.R., Ritter, P., Jirsa, V.K., Deco, G., 2015. The rediscovery of slowness: exploring the timing of cognition. TICS 19, 616–628.
Kuramoto, Y., 1984. Chemical Oscillations,Waves, and Turbulence. Springer-Verlag, Berlin.
Kuznetsov, Y.A., 1998. Elements of Applied Bifurcation Theory. Springer, New York.
Litvak, V., Komssi, S., Scherg, M., Hoechstetter, K., Classen, J., Zaaroor, M., Pratt, H., Kahkonen, S., 2007. Artifact correction and source analysis of early electroencephalographic responses evoked by transcranial magnetic stimulation over primary motor cortex. NeuroImage 37, 56–70.
Lord, L.-D., Stevner, A.B., Deco, G., Kringelbach, M.L., 2017. Understanding principles of integration and segregation using whole-brain computational connectomics: implications for neuropsychiatric disorders. Philos. Trans. R. Soc. A Math. Phys. Eng. Sci. 375.
Massimini, M., Ferrarelli, F., Huber, R., Esser, S.K., Singh, H., Tononi, G., 2005. Breakdown of cortical effective connectivity during sleep. Science 309, 2228–2232.
Mohseni, H.R., Smith, P.P., Parsons, C.E., Young, K.S., Hyam, J.A., Stein, A., Stein, J.F., Green, A.L., Aziz, T.Z., Kringelbach, M.L., 2012. MEG can map short and long-term changes in brain activity following deep brain stimulation for chronic pain. PLoS One 7, e37993.
Muldoon, S.F., Pasqualetti, F., Gu, S., Cieslak, M., Grafton, S.T., Vettel, J.M., Bassett, D.S., 2016. Stimulation-based control of dynamic brain networks. PLoS Comput. Biol. 12, e1005076.
Pereda, E., Gamundi, A., Rial, R., Gonzalez, J., 1998. Non-linear behaviour of human EEG: fractal exponent versus correlation dimension in awake and sleep stages. Neurosci. Lett. 250, 91–94.
Pikovsky, A., Rosenblum, M., Kurths, J., 2003. Synchronization: a Universal Concept in Nonlinear Sciences. Cambridge University Press, Cambridge.
Ponce-Alvarez, A., Deco, G., Hagmann, P., Romani, G.L., Mantini, D., Corbetta, M., 2015. Resting-state temporal synchronization networks emerge from connectivity topology and heterogeneity. PLoS Comput. Biol. 11, e1004100.
Pradhan, N., Sadasivan, P.K., 1996. The nature of dominant Lyapunov exponent and attractor dimension curves of EEG in sleep. Comput. Biol. Med. 26, 419–428.
Raichle, M.E., 2009. A brief history of human brain mapping. Trends Neurosci. 32, 118–126.
Raichle, M.E., MacLeod, A.M., Snyder, A.Z., Powers, W.J., Gusnard, D.A., Shulman, G.L., 2001. A default mode of brain function. Proc. Natl. Acad. Sci. U. S. A. 98, 676–682.
Rissman, J., Gazzaley, A., D'Esposito, M., 2004. Measuring functional connectivity during distinct stages of a cognitive task. NeuroImage 23, 752–763.
Rosanova, M., Gosseries, O., Casarotto, S., Boly, M., Casali, A.G., Bruno, M.A., Mariotti, M., Boveroux, P., Tononi, G., Laureys, S., Massimini, M., 2012. Recovery of cortical effective connectivity and recovery of consciousness in vegetative patients. Brain A J. Neurol. 135, 1308–1320.
Saenger, V.M., Kahan, J., Foltynie, T., Friston, K., Aziz, T.Z., Green, A.L., van Hartevelt, T.J., Cabral, J., Stevner, A.B.A., Fernandes, H.M., Mancini, L., Thornton, J., Yousry, T., Limousin, P., Zrinzo, L., Hariz, M., Marques, P., Sousa, N., Kringelbach, M.L., Deco, G., 2017a. Uncovering the underlying mechanisms and whole-brain dynamics of deep brain stimulation for Parkinson's disease. Sci. Rep. 7, 9882.
Saenger, V.M., Ponce-Alvarez, A., Adhikari, M., Hagmann, P., Deco, G., Corbetta, M., 2017b. Linking entropy at rest with the underlying structural connectivity in the healthy and lesioned brain. Cereb. cortex 1–11.
Siebner, H.R., Bergmann, T.O., Bestmann, S., Massimini, M., Johansen-Berg, H., Mochizuki, H., Bohning, D.E., Boorman, E.D., Groppa, S., Miniussi, C., Pascual-Leone, A., Huber, R., Taylor, P.C., Ilmoniemi, R.J., De Gennaro, L., Strafella, A.P., Kahkonen, S., Kloppel, S., Frisoni, G.B., George, M.S., Hallett, M., Brandt, S.A., Rushworth, M.F., Ziemann, U., Rothwell, J.C., Ward, N., Cohen, L.G., Baudewig, J., Paus, T., Ugawa, Y., Rossini, P.M., 2009. Consensus paper: combining transcranial stimulation with neuroimaging. Brain Stimul. 2, 58–80.
Smith, S.M., Fox, P.T., Miller, K.L., Glahn, D.C., Fox, P.M., Mackay, C.E., Filippini, N., Watkins, K.E., Toro, R., Laird, A.R., Beckmann, C.F., 2009. Correspondence of the brain's functional architecture during activation and rest. Proc. Natl. Acad. Sci. U. S. A. 106, 13040–13045.

Spiegler, A., Hansen, E.C., Bernard, C., McIntosh, A.R., Jirsa, V.K., 2016. Selective activation of resting-state networks following focal stimulation in a connectome-based network model of the human brain. eNeuro 3.
Stam, C.J., 2005. Nonlinear dynamical analysis of EEG and MEG: review of an emerging field. Clin. Neurophysiol. Off. J. Int. Fed. Clin. Neurophysiol. 116, 2266–2301.
Tagliazucchi, E., Laufs, H., 2014. Decoding wakefulness levels from typical fMRI resting-state data reveals reliable drifts between wakefulness and sleep. Neuron 82, 695–708.
Tononi, G., Edelman, G.M., Sporns, O., 1998. Complexity and coherency: integrating information in the brain. Trends Cognit. Sci. 2, 474–484.
Tzourio-Mazoyer, N., Landeau, B., Papathanassiou, D., Crivello, F., Etard, O., Delcroix, N., Mazoyer, B., Joliot, M., 2002. Automated anatomical labeling of activations in SPM using a macroscopic anatomical parcellation of the MNI MRI single-subject brain. NeuroImage 15, 273–289.
Van Nes, E.H., Scheffer, M., 2007. Slow recovery from perturbations as a generic indicator of a nearby catastrophic shift. Am. Nat. 169, 738–747.
Vasa, F., Shanahan, M., Hellyer, P.J., Scott, G., Cabral, J., Leech, R., 2015. Effects of lesions on synchrony and metastability in cortical networks. NeuroImage 118, 456–467.
Wissel, C., 1984. A universal law of the characteristic return time near thresholds. Oecologia 65, 101–107.
Yarkoni, T., Poldrack, R.A., Nichols, T.E., Van Essen, D.C., Wager, T.D., 2011. Large-scale automated synthesis of human functional neuroimaging data. Nat. Methods 8, 665–670.
Zhang, D., Raichle, M.E., 2010. Disease and the brain's dark energy. Nat. Rev. Neurol. 6, 15–28.